

A unified mechanism for conductivity and magnetism at interfaces of insulating nonmagnetic oxides

Liping Yu^{1,2} and Alex Zunger¹

1 University of Colorado, Boulder, Colorado 80309, USA

2 National Renewable Energy Laboratory, Golden, CO 80410, USA

The conducting two-dimensional electron gas (2DEG) and magnetism formed at the interface between insulating nonmagnetic oxides, as exemplified by polar LaAlO₃ (LAO) and nonpolar SrTiO₃ (STO) has raised prospects for attaining interfacial functionalities absent in the component materials. Yet, the microscopic origin of such emergent phenomena remains unclear. Using first principles defect theory, here we find a general mechanism that simultaneously resolves the leading puzzles and their related experimental observations, identifying the agents for creation and compensation of itinerant charge carriers and interface magnetism. We demonstrate that the polar-discontinuity-induced electric field in the LAO film triggers thermodynamically the spontaneous formation of surface defects at some critical film thickness. The electrons ionized from these surface donors are transferred by the internal electric field to the STO creating a 2DEG and, at the same time, setting up counter field that resolves the divergence of built-up electric potential. The Al-on-Ti anti-site acceptor at the interface traps part of the 2DEG, whereas the Ti-on-Al anti-site donor can lead to interface magnetism. Our results provide practical routes for inducing and controlling both conductivity and magnetism at oxides interfaces.

Oxide interfaces exhibit many spectacular phenomena not found in the respective bulk components or in conventional semiconductor interfaces¹, providing new avenues for novel electronics^{2,3}. The LAO/STO interface is a leading example, exhibiting conducting 2DEG^{4,5}, ferromagnetism⁶⁻¹², and superconductivity¹³ and between two insulating nonmagnetic metal-oxides. The emergent 2DEG and magnetism might be two most intriguing properties that have attracted widespread study. However, despite years of extensive effort, their microscopic origin and controlling factors are yet unclear and lie at the heart of numerous controversies^{14,15}.

Along the (001) direction, the III-III-O₃ perovskite such as LAO is polar, consisting of alternating, oppositely charged layers of $(\text{La}^{3+}\text{O}^{2-})^+$ and $(\text{Al}^{3+}\text{O}_2^{2-})^-$, whereas II-IV-O₃ perovskites such as STO is nonpolar, consisting of alternating charge-neutral layers of $(\text{Sr}^{2+}\text{O}^{2-})^0$ and $(\text{Ti}^{4+}\text{O}_2^{2-})^0$. The growth of polar layers on a non-polar substrate could then lead to an impending electrostatic divergence. A key question is what types of charge rearrangement preempt the electrostatic divergence of the built-up electric potential as the thickness of the polar LAO film increases. The prevalent model is intrinsic electronic reconstruction (so called polar catastrophe, or PC) involving ionization of the host valence band of LAO within the abrupt and defect-free interfaces^{4,5,16,17}. The other mechanisms based on structural imperfections have also been proposed, including the oxygen vacancies $\text{V}_\text{O}(I)$ at the interface (*I*) within the STO substrate¹⁸⁻²⁰, the $\text{V}_\text{O}(S)$ at LAO film surface (*S*)²¹⁻²⁴, and the intermixing of cations across the interface^{16,25-31}. Each factor alone represents a single aspect of the interface physics, explains some experimental findings, but conflicts with a few others (See Table 1 in extended Data). For interface magnetism, the local moments have been postulated to arise either from interfacial disorder^{32,33}, or are related to oxygen vacancies³⁴. It is even unclear whether the magnetism resides in STO or LAO side. Whether or how the local magnetic moments interact with the 2DEG is another unresolved issue¹¹.

Using first-principles electronic structure and defect theory^{35,36}, we examine systematically and

critically the previously proposed mechanisms and build upon them. The key physical quantities that feature in our explanation are (i) the defect formation energy $\Delta H(q, E_F, \{\mu\})$, which is a function of the defect charge state q , the Fermi-energy E_F , and the chemical potential $\{\mu\}$ of atoms that comprise the defect (reflecting the growth conditions). The magnitude of ΔH controls the defect concentration. (ii) The donor or acceptor electrical levels, i.e., the defect charge transition energy $\varepsilon(q/q')$ defined as the E_F where the ΔH of a defect at two different charge states q and q' equal. (Note this quantity reflects differences in total energies, not single-particle levels). A donor level produces electrons and compensates holes, whereas an acceptor level produces holes and compensates electrons. (iii) The thermodynamic equilibrium E_F under a given growth condition, which is established as a balance of all electrons and holes concentrations contributed by thermal ionization of all considered defects. Details of the first principles calculations of these quantities are given in Method Summary. Our calculation differs in some key aspects from previous defect calculations on this system. Previous calculations^{21-24,28,31,34,37,38} either (a) postulated the existence of certain defects without examining thermodynamic quantities such as $\Delta H(q, E_F, \{\mu\})$ that decide if a defect exist in reasonable concentration to have any electrical consequence or (b) considered ΔH only for the charge *neutral* defect states (which do not create carriers) allowing a chemically unconstrained broad range of chemical potentials $\{\mu\}$ that is unlikely to be achievable in experiment. Hence, the electrical transition levels $\varepsilon(q/q')$ and the thermodynamic equilibrium E_F , which decide the defect electrical activity and ΔH , still remain unexplored.

A central result of this work is that the *thermodynamics* of formation of some defects depends critically on the built-in electric field induced by polar-discontinuity. Usually the formation of defects in solids requires an energy investment, so the ground state structure of a crystal can be defect free. In the present case, however, the built-in electric field in the polar film reduces the energy ΔH required to form certain defects (e.g., V_O) at its surface or certain defect pairs (e.g., $Ti \leftrightarrow Al$ exchanged pair) across the interface. This triggers at some defect-dependent critical thickness (L_c) the *spontaneous (exothermic) formation of surface* defects that would otherwise require high energy to form in the corresponding *bulk*. *Thus, the stable ground state structure of this system is not defect-free*. The specific ensuing defects that we find to be abundant are then responsible for the creation and compensation of carriers and for interface magnetism. The key role of polar-discontinuity here is that it induces a built-in electric field in the polar film that enables long-distance charge transfer in a direction that sets up an opposite dipole, which in turn cancels the built-in electric field that has created the defects in the first place. Once the electric field in the polar film is cancelled, the ΔH of the field-induced defects returns to its initial large value like in the bulk. Without such a polar-discontinuity-induced built-in field, the long-distance charge transfer would not occur since it will create a large dipole that will increase the electrostatic energy proportional to that dipole.

The emerging unified mechanism for 2DEG and magnetism at STO/LAO interfaces is illustrated in **Figure 1**. For ***n*-type** interfaces (i.e., LAO grown on TiO_2 -terminated STO substrate), there exists an LAO critical thickness (L_c) of ~ 4 unit cells (uc), below which the anti-site defect pair $Al_{Ti}(I)+Ti_{Al}(S)$ created by $Ti \leftrightarrow Al$ exchange across the interface forms spontaneously (Fig.1a). These pair defects set up opposite dipoles that compensate largely the built-in electric field in LAO, without inducing free carriers. This explains the experimentally observed weak electric field in LAO even below the L_c , which cannot be reconciled within the PC scenario. Above the L_c , the $V_O(S)$ form spontaneously and donates electrons that are transferred by the built-in electric field to the interface (Fig.1b). The part of the resulting interface 2DEG is trapped mainly by the Al-on-Ti (Al_{Ti}) defect, which has a deep electrical acceptor level and is abundant. Once the built-field has been largely cancelled by $V_O(S)$ -induced charge transfer, the $Ti \leftrightarrow Al$ exchanged defect pair and V_O in LAO can barely form further. The Ti ions that substitute Al ions (i.e. charge neutral Ti_{Al} defects) stay in 3+ oxidation states and can induce interface magnetism. ***For p-type*** interfaces (i.e., LAO grown on SrO -terminated STO substrate),

there also exists an L_c , below which the $\text{La} \Leftrightarrow \text{Sr}$ exchanged pair defects, i.e., $\text{La}_{\text{Sr}}(I) + \text{Sr}_{\text{La}}(S)$, form spontaneously (Fig.1c), and above which the $\text{La}_{\text{Sr}}(I)$ and $\text{V}_{\text{La}}(S)$ form spontaneously as defect complex (Fig.1d). Such defect pairs and complexes form opposite dipoles and compensate the electric field in LAO. On the other hand, they also produce no free carriers at both interface and surface regions (whence insulating).

We next explain more specifically how this mechanism resolves the main outstanding puzzles¹⁵ and identifies the design principles for controlling both conductivity and magnetism at the interface.

What creates the 2DEG?

The PC model identifies the source of 2DEG electrons as being the ionization of the LAO VBM (**Figure 2a**). This also predicts that the LAO free surface would be hole conducting, conflicting with the measured insulating surface seen in experiment^{4,5}.

The interface $\text{V}_0(I)$ within STO¹⁸⁻²⁰, the surface $\text{V}_0(S)$ in LAO²¹⁻²⁴, and the interfacial La_{Sr} defects^{16,30,37}, have also been proposed as possible sources of the 2DEG. Our results in **Figure 3a** show that the interfacial point donor defects (La_{Sr} , Ti_{Al} , and V_0) do not contribute to the 2DEG when one considers the correct equilibrium E_F : Indeed, for any LAO film thickness (n_{LAO}), the calculated equilibrium E_F of the system stays within the upper half of the STO band gap (shaded area in Fig.3a). Consequently, the individual La_{Sr} and Ti_{Al} antisite defects do not produce carriers (because their donor electrical levels are too deep in the gap, hence not ionizable), nor does the interfacial $\text{V}_0(I)$ exist in any significant amount (even though its donor level is shallow, its ΔH is too high so its concentration is too low). Thus, contrary to earlier postulations, these defects do not contribute to 2DEG, consistent with recent experiments³¹.

In contrast with the ΔH of the $\text{V}_0(I)$, **Figure 4a** shows the ΔH of the surface vacancy $\text{V}_0(S)$ decreases linearly as n_{LAO} increases, consistent with previous calculations^{24,38}. When the ΔH becomes zero (or close to zero) at $n_{\text{LAO}} \sim 4$ uc, the $\text{V}_0(S)$ will form spontaneously. Fig. 3 indicate that the V_0 defects in different layers across the interface have almost same electrical donor level, which is higher than the STO conduction band edge at the interface due to band bending effect. This suggests that the donor level of surface V_0 is also higher in energy than the STO conduction band edge at the interface. As a result, the electrons ionized from the formed $\text{V}_0(S)$ will be transferred by the built-in electric field to the interface, forming 2DEG there. Such electron transfer cancels the built-in electric field and bringing the LAO valence bands back to well below the STO conduction bands. Hence the $\text{V}_0(S)$ defects cause 2DEG at the interface, but do not induce free holes at the LAO surface (whence insulating).

The emerging design principle for selecting materials that will likely form interface 2DEG is that the electrical donor level at the surface of the polar material be higher in energy than the conduction band edge of the nonpolar substrate at the interface. If this condition is satisfied, the existence of polar-discontinuity-induced built-in electric field in the polar film will enable the charge transfer from such surface donor state to the conduction band of nonpolar material across the LAO film, in a direction that can set up an opposite dipole, which in turn cancels the built-in electric field. This picture suggests that the 2DEG at n-type STO/LAO interfaces can also be induced and/or tuned by using some surface adsorbates (e.g., H_2O , H)³⁹⁻⁴¹ or metallic contacts⁴² if the ionization energy of the surface adsorbate (or the work function of the metallic contact) is not lower than the STO conduction band edge at the interface.

What controls the critical thickness?

The key argument in favor of the PC mechanism is its predicted critical thickness (L_c) of metal-insulator transition. Both electrostatics and the first principles calculations based on density functional theory (DFT) with the generalized gradient approximation (GGA)⁴³, shown in Fig 2c lead to an L_c between three and four unit cells^{17,44}. However, these results may be clouded by specific uncertainties:

the electrostatic model depends on the choice of the LAO film dielectric constant and LAO/STO band offsets, whereas the GGA calculation suffers from the well-known band gap underestimation problem⁴⁵. To examine this point we have applied the HSE hybrid functional⁴⁶, which predicts correctly the experimental bulk STO band gap of 3.2 eV. We find an L_c of 4-5 uc (Fig 2c)). It is noteworthy that, for $n_{LAO} = 4$ uc, the band gap of the system turns out to be 1.1 eV, suggesting an insulating behavior, contrasting with the experiment where the robust conductivity has been observed at this thickness. Hence, strictly speaking, the defect-free polar catastrophe model cannot explain the L_c either⁴⁷.

The field-assisted formation of $V_O(S)$ naturally explains the L_c of metal-insulator transition. Fig.4a shows that ΔH of $V_O(S)$ becomes zero above a critical thickness of $L_c = 4$ uc under a typical O-rich growth condition. For the LAO film that is one unit cell thinner than this L_c , the calculated ΔH of $V_O(S)$ is 0.75 eV -- too high to produce significant free carrier concentration. Thus, the appearance of $V_O(S)$ (and the metal-insulator transition) at L_c is sharp. Note that the calculated slope $\Delta H/n_{LAO}$ is 0.19 eV/Å, equal to the calculated built-in electric field E in LAO (Supplementary discussion). The suggested L_c is then controlled by the ΔH of a V_O at the interface (ΔH_o) and the built-in electric field (E_{in}) in LAO film via $L_c = \Delta H_o/eE_{in}$. For the annealed interface samples, the resulting L_c stays around 4 uc (Extended Data Figure 2 and supplementary discussion), consistent with experiment^{4,5}. More specifically, this L_c can be estimated by $L_c = \Delta H_o \epsilon / 4\pi e P_0$, since $E_{in} = 4\pi P_0 / \epsilon$, where ϵ and P_0 are the dielectric constant and nominal polarization of LAO film. This relation explains the variation of the L_c with the fraction x in $(LAO)_{1-x}(STO)_x$ overlayer (where P_0 is proportional to x).

Implication on carrier mobility: the relatively high 2DEG mobility is essentially enabled by a modulated doping effect⁴⁸, whereby the source of carriers (LAO surface) is spatially separated from the place where they reside (LAO/STO interface), thus minimizing carrier scattering by ionized defects. This minimal spatial separation is measured by the L_c . The design principles suggested from $L_c = \Delta H_o \epsilon / 4\pi e P_0$ for achieving a large L_c (hence maintaining good mobility) is to find polar materials with small polarization, large dielectric constant, and shallow donor defects with high- ΔH (which also depends on the growth condition) in bulk or at the polar-nonpolar interface.

What compensates the built-in electric field?

In a *defect-free* interface structure, both previous DFT-GGA calculations^{24,49} and our HSE calculation (Fig.2d) predict a large electric field of 0.19 V/Å in the LAO film of $n_{LAO} < L_c$, which decreases gradually as n_{LAO} increases for $n_{LAO} \geq L_c$, approaching zero only at infinitely thick n_{LAO} . This prediction of the PC model conflicts with experiments, where only very weak residual field has been observed for all investigated n_{LAO} ⁵⁰⁻⁵³. The weak electric field for $n_{LAO} \geq L_c$ is naturally explained by the surface $V_O(S)$ model: the spontaneously formed (hence, abundant) $V_O(S)$ defects donate electrons being transferred to the interface, reducing the electric field drastically in LAO film. However, for $n_{LAO} < L_c$ where $V_O(S)$ is barely present, such weak field cannot be explained.

To explain the weak electric field in LAO film below the L_c , we examined the role of the cation mixing across the interface. For $n_{LAO} < L_c$, previous first-principles calculation³⁷ found that the energy required to form the antisite defect pair $[Al_{Ti}+Ti_{Al}]$ via a $Ti \leftrightarrow Al$ exchange is negative (i.e., exothermic), and the largest energy gain is obtained when a Ti atom of TiO_2 -interface layer is exchanged with an Al of AlO_2 -surface layer, i.e., $Al_{Ti}(I)+Ti_{Al}(S)$ ³⁷. Our calculation for $n_{LAO} = 4$ uc (Fig.4b) shows the same feature. This stability is understandable since the Ti_{Al} electrical donor level is higher in energy than the Al_{Ti} electrical acceptor defect (cf. Fig.1a and Fig.3a), and the electrons can transfer from the former to the latter via the built-in electric field in LAO. This charge transfer in turn creates opposite dipole, compensating the built-in electric field in LAO film below the L_c . Such antisite defect pairs if formed above the L_c do not lead to field compensation for two reasons: one is that the formation of $V_O(S)$ in this case prevents or reduces the further formation of the $Ti \leftrightarrow Al$ exchanged pair defects across the

interface (Fig. 4b); The other is that the electron transfer from $V_O(S)$ to the interface is energetically more stable than from $Ti_{Al}(S)$ to the interface, since $V_O(S)$ has a higher electrical donor level than Ti_{Al} (Fig.1b).

What reduces the interfacial carrier density?

The total charge (mobile and immobile) that corresponds to zero electric field in LAO is 0.5 e/S (where S is 2D unit cell area), according to Gauss's law in electrostatics. However, electrically, the measured sheet carrier density in annealed sample is always about an order of magnitude smaller than 0.5 e/S. This reduction cannot be explained by PC model that predicts interfacial charge densities significantly larger than experimental values (Fig.2e). The possibility of multiple types of interfacial carriers that occupy different subbands (d_{xy} , d_{xz}/d_{yz}) has also been suggested.⁵⁴⁻⁵⁷ However, it is debatable, since it is hard to reconcile within this picture why the full carrier density of 0.5 e/S could be observed at $GdTiO_3/STO$ interfaces⁵⁸ (where the same multiple carrier types exist) and why the Ti d_{xy} electrons (localized along z-direction out of the interface, but very delocalized along the x/y-direction within the interface plane⁵⁶) should not contribute to the transport in the xy-plane.

Such interfacial *carrier reduction* is naturally explained by defect physics. Fig. 3a shows that above L_c , when the E_F is high in the gap, the electron-trapping Al_{Ti} antisite and the cation vacancies (V_{Sr} and V_{Ti}) within STO at the interface have low formation energy ΔH in their charged states. The Al_{Ti} anti-sites are more abundant than the metal vacancies V_{Sr} and V_{Ti} since their ΔH is significantly lower than that of the vacancies at most E_F that are possible during the layer-by-layer epitaxial growth. Hence the Al_{Ti} acceptors are the most potent source of electron trapping leading to a lower interfacial carrier density. On the other hand, Fig.4b indicates that the spontaneously formed $V_O(S)$ above L_c , prevents further the formulation of the $Ti \leftrightarrow Al$ exchanged pairs (not considered in Fig.3a) that also result in $Al_{Ti}(I)$ defects. As a result, the $Al_{Ti}(I)$ defects generally cannot form in sufficient amount to trap all 0.5e/S 2DEG there, which leads to significantly reduced carrier density.

Implication on carrier density: The above picture suggests that the main controlling factor for the interface carrier density is the concentration of the deep acceptor defects (mainly Al_{Ti}), which should be minimized for achieving high carrier density. On the other hand, it means that if sufficient concentration of deep acceptor defects form at the interface, the itinerant charge carrier can be trapped completely, leading to insulating behavior. This might be case in the insulating n-type interfaces with La-rich off-stoichiometric LAO films^{31,59}, where additional V_{Al} acceptors could diffuse to the interface and cause additional electron-trapping V_{Sr} and V_{Ti} defects at the interface³¹.

What causes interface magnetism?

The interface magnetism observed at n-type interfaces⁸⁻¹⁰ is another remarkable emergent phenomenon, which is unexpected since both STO and LAO are nonmagnetic in bulk. Recent experiments illustrated that the ferromagnetic order at the interface has Ti^{3+} character (here 3+ refers to oxidation state not to donor charge state) in the d_{xy} orbital of the anisotropic t_{2g} band, and appears at the same critical thickness L_c of conductivity⁸⁻¹⁰. It is puzzling that the Ti^{3+} oxidation state signals have also been detected below the critical thickness^{52,60}, where neither magnetism nor conductivity appear. Theoretically, several sources (e.g., interface disorder^{32,33}, or interfacial oxygen vacancies³⁴) for local magnetic moment have been postulated and are still under debate.

The defect picture identified here offers an alternative explanation for such interface magnetism. We found that before the built in field has been cancelled, the antisite Ti_{Al} formed in LAO is ionized (i.e, the oxidation state of Ti is Ti^{4+}) whereas after the field has been cancelled the anti site defect Ti_{Al} is not ionized (i.e., the oxidation state of Ti is Ti^{3+}). The former situation arises because the electrons ionized from Ti_{Al} defects can transfer to the interface via built-in electric field. The latter situation arises because the ionized electrons of Ti_{Al} defect cannot travel to a distance far way for it, since the resulting

dipole will increase the electrostatic energy proportionally and destabilize the system. Below the L_c , the excess Ti_{Al} defects can be induced at or below the LAO surface layer, due to the small ΔH (Fig. 3), after the built-in electric field in LAO has been largely cancelled by the spontaneously formed $[\text{Ti}_{\text{Al}}(S)+\text{Al}_{\text{Ti}}(I)]$ pair defects. These unionized excess Ti_{Al} defects thus explains to the Ti^{3+} signals observed below the L_c . Above the L_c , all formed interfacial Ti_{Al} defects become ionized and exhibit localized Ti^{3+} characters, since the $\text{V}_\text{O}(S)$ defects readily cancel the electric field in LAO.

The local magnetic moment of a single such defect at the interface may be estimated from that in bulk LAO (where the electric field is zero), which is $0.84\mu_B$ from our hybrid functional calculation. Thus, for $\text{Ti } d_{xy}$ ferromagnetic order, the total magnetic moment of the interface depends on the concentration of unionized Ti_{Al} (i.e., Ti^{3+} -on- Al^{3+}) defects in LAO and can be very small per atom on average. Below the L_c , the excess Ti^{3+} -on- Al^{3+} defects have a much smaller concentration than the ionized $\text{Ti}_{\text{Al}}(S)$ (i.e., Ti^{4+} -on- Al^{3+}) defects caused by the thermodynamic $\text{Ti} \rightleftharpoons \text{Al}$ atom exchanges, and the magnetism due to the excess Ti^{3+} there may not be detectable. While above the L_c , the Ti atoms become almost exclusively $4+$ in LAO due to presence of the $\text{V}_\text{O}(S)$ defects, leading to measurable magnetism. Hence, the L_c for the appearance of magnetism suggested here is same as that for conductivity, consistent with experiments.⁸⁻¹⁰ Since the charge associated with deep Ti^{3+} -on- Al^{3+} defect is very localized, the appearance of such defects (i.e., Ti^{3+} signals) below the L_c does not induce conductivity, consistent with experiment. Above the L_c , the Ti^{3+} -on- Al^{3+} related carrier also explains well the observed Ti^{3+} -type charge carrier centered at around the middle of STO band gap and independent of the oxygen pressure during the growth⁶¹.

The route suggested from above for enhancing the interface ferromagnetism here thus is to increase the concentration of deep Ti_{Al} defect in the LAO film. This local moment nature is similar to the Ti -dopant in bulk LAO where no internal field exists. One special feature here is the Ti_{Al} defects are confined near the interface within LAO side, and the resulting magnetic property has 2D character, which might be good for nanoscale device application.

Why are p-type interfaces insulating?

In the PC scenario for p-type interface structure, hole conducting interface and electron conducting surface are expected when STO valence band overlaps the LAO conduction bands (Fig.2b). However, no conductivity has been observed in both regions in experiment^{4,5}. To understand this perplexing insulating behavior, hole-polaron model⁶² and hole-compensating interfacial V_O model^{16,38} have been postulated. Both models focus only on the interface free of cation intermixing, and assume that holes preexist at the interface and originate from the intrinsic valence bands there. Neither can explain the insulating behavior at the surface. In following, we find that the insulating nature of p-type interfaces is due to the spontaneously formed defect pairs or complexes that compensate the built-in electric field in LAO but induce no free carriers.

Our results in Fig.4c,d suggest that the built-in electric field in LAO film is always compensated by the defect complexes. Fig.4c shows that the ΔH of “surface $\text{V}_{\text{La}}(S)+$ interfacial $\text{La}_{\text{Sr}}(I)$ ” defect complex decreases linearly as n_{LAO} increases, and become zero at a critical thickness (L_c) of ~ 4 uc. It means that such defect complex will form spontaneously when $n_{\text{LAO}} \geq L_c$. Below the L_c , due to the absence of surface V_{La} defects, Fig.4d indicates that the defect pairs $[\text{La}_{\text{Sr}}(I)+\text{Sr}_{\text{La}}(S)]$ caused by $\text{La} \rightleftharpoons \text{Sr}$ exchange across the interface have negative ΔH and can thus form spontaneously. The built-in electric field in LAO below and above the L_c is then cancelled by $[\text{La}_{\text{Sr}}(I)+\text{Sr}_{\text{La}}(S)]$ defect pairs and $[\text{V}_{\text{La}}(S)+\text{La}_{\text{Sr}}(I)]$ defect complexes, respectively. The reason for such feature is that the electric donor level of La_{Sr} is higher than the electrical acceptor levels of V_{La} and Sr_{La} (Fig.3b), the electrons ionized from the former will thus be transferred to the latter by the built-in electric field, setting up opposite dipoles that in turn compensate the built-in electric field. For $n_{\text{LAO}} \geq L_c$, the electron transfer from $\text{La}_{\text{Sr}}(I)$ to $\text{V}_{\text{La}}(S)$ is more favorable than that from $\text{La}_{\text{Sr}}(I)$ to $\text{Sr}_{\text{La}}(S)$, since $\text{V}_{\text{La}}(S)$ has a lower electrical acceptor level than

$V_{La}(S)$. The complete compensation of the built-in electric field in LAO means that the LAO conduction bands never cross the LAO valence bands for any n_{LAO} and hence no free carriers can be induced at both interface and surface regions.

The results in Fig.3b shows that the point defects at p-type interfaces do not contribute itinerant carriers either. For any n_{LAO} , since the built-in electric field in LAO is always compensated, the resulting E_F due to the interfacial point defects is always pinned around 0.7 eV below the STO CBM for $n_{LAO} = 2$ uc. Around this pinning E_F , Fig. 3b shows that interfacial La_{Sr} and Ti_{Ar} donor defects are not ionized, though having low ΔH . The other interfacial defects (such as V_O , Sr_{La} , Al_{Ti} and cation vacancies) have rather high ΔH and they are unlikely form to induce itinerant electrons and holes at the interface.

Discussion

The emerging mechanism establishes the connection between the polar discontinuity and the defects, resolves the leading puzzles, and explains a set of critical experimental observations (Extended Data Table 1) associated with these puzzles. A most important feature is that the formation of donor-acceptor defect pairs caused by $Ti \leftrightarrow Al$ exchange across n-type interfaces and by $La \leftrightarrow Sr$ across p-type interfaces is exothermic and may be inevitable before the polar-discontinuity-induced electric field in LAO has been cancelled. These deep defect pairs do not induce itinerant carriers by themselves, but can trap itinerant carriers there. On the other hand, they are also detrimental for carrier mobility. This situation brings experimental challenges on how to reduce the concentration of defect pairs for enhancing both the carrier density and mobility in this STO/LAO system. According to this unified mechanism, this challenge may be addressed by designing other oxide interfaces that have corresponding donor-acceptor pairs with the donor level lower than the acceptor level.

This mechanism favors $V_O(S)$ as the source of interface 2DEG. To validate it further, our results suggest performing more direct and precise experimental measurements on V_O for the interfaces with LAO film right below or above the L_c . For interface magnetism, this mechanism favors the Ti_{Al} defects in LAO near the interface as the source for local moments. How these local moments are ordered (ferromagnetic, or antiferromagnetic, or else) and whether/how they can interact with the itinerant 2DEG should be investigated further.

Methods Summary

The calculations were performed using DFT and plane-wave projector augmented-wave (PAW)⁶³ method as implemented in the VASP code⁶⁴. An energy cutoff of 400 eV was used. The Brillouin zone was sampled by $8 \times 8 \times 1$ and $4 \times 4 \times 1$ \mathbf{k} -point mesh for 1×1 and 2×2 in-plane supercell respectively. The atomic forces were relaxed to be less than 0.03 eV/Å. The in-plane lattice constant was fixed to 3.943 Å (the GGA relaxed lattice constant of STO). In slab calculations, the 4 uc (\sim 16 Å) vacuum layer was used and the dipole correction was always applied to remove artificial dipole interactions⁶⁵. The electric field in LAO center (Fig.2d) was calculated as the derivative of macroscopic planar-averaged electrostatic potential using saw-tooth weight function⁶⁶.

The formation energy of a defect is a function of defect charge state, the Fermi-energy and the chemical potential of atoms that comprise the defect. It was calculated by using the method described in Ref.³⁵. In Fig.3, the total energy and electronic structure of interfaces were calculated by using HSE hybrid functional on the top of the GGA relaxed structures. The equilibrium Fermi-energy was calculated self-consistently according to charge neutrality condition⁶⁷. In Fig.4, all results were obtained from GGA. The chemical potentials relative to their elemental solid (or gas) phase are taken as variables and are bounded by the values that maintain a stable host compound and avoid formation of other competing phases (Al_2TiO_5 , SrAl_2O_4 , La_2TiO_5 , $\text{La}_2\text{Ti}_2\text{O}_7$, LaTiO_3 , Al_2O_3 , La_2O_3 , SrO , TiO_2) in thermodynamic equilibrium³⁶. The experimental (T , P_{O_2}) conditions for growing (or annealing) an oxide material were calculated from the relative oxygen chemical potential according to the thermodynamic model⁶⁸.

Acknowledgements

This work was supported as part of the Center for Inverse Design, an Energy Frontier Research Center funded by the U.S. Department of Energy, Office of Science, Basic Energy Sciences under the contract No. DE-AC36-08GO28308 to National Renewable Energy Laboratory (NREL). The computation was done by using capabilities of the NREL Computational Sciences Center supported by the U.S. DOE office of Energy Efficiency and Renewable Energy, under Contract No. DE-AC36-08GO28308.

Author Contributions

L.Y. carried out the calculations, analyzed the results and wrote the paper. A.Z. contributed to the analysis of results and the writing of the paper.

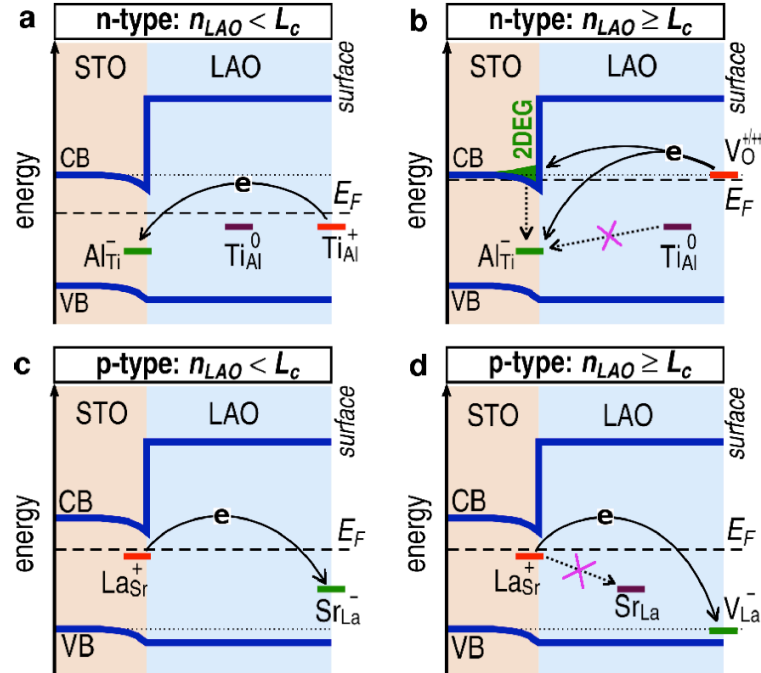


Figure 1: Schematic band diagram and defect levels within the unified mechanism. **a,b**, n-type interfaces with n_{LA0} below and above the critical thickness (L_c) of metal-insulator transition (i.e., the spontaneous formation of O vacancies at the LAO surface). **c,d**, p-type interfaces with n_{LA0} below and above the critical thickness of spontaneous formation of La vacancies (V_{La}) at the LAO surface. The superscripts (0, +, ++, -) denote the defect charge states, not the oxidation states of the ions there.

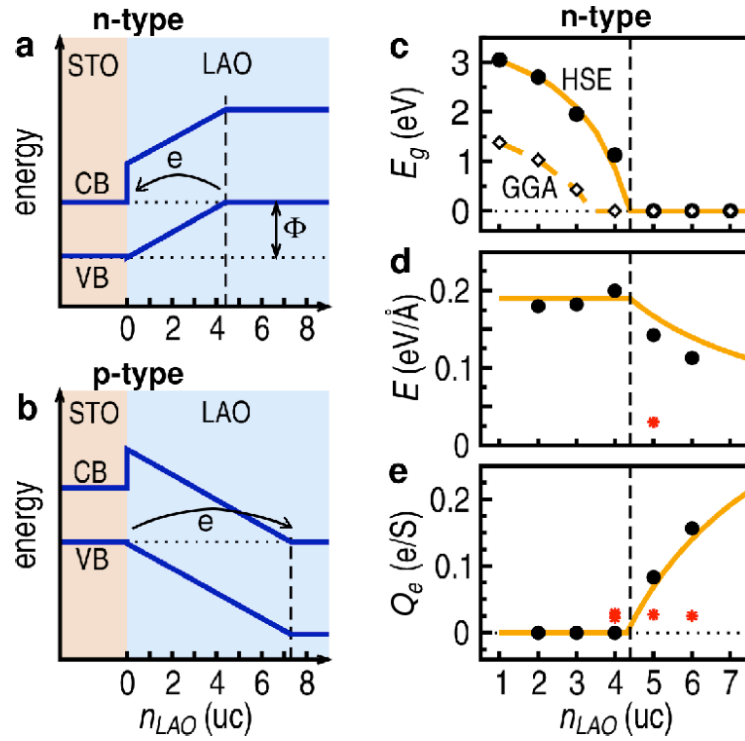


Figure 2: Electronic properties of abrupt defect-free interfaces within the polar catastrophe scenario. **a,b**, schematic band diagram for n-type and p-type interfaces respectively. **c**, GGA and HSE band gaps of 6STO/ n LAO/vacuum interfaces. **d**, Calculated macroscopic planar-averaged electric field in the center of LAO film by HSE. The experimental data (*) is taken from ref.⁵¹. **e**, Calculated interfacial carrier density: HSE (black dots) vs. experiment (red stars)⁵. The orange lines in **d,e** are calculated from the simple electrostatic model using $\Phi=3.3$ eV (see **a**) and the LAO film dielectric constant of 30, suggesting a critical thickness of 4.3 uc.

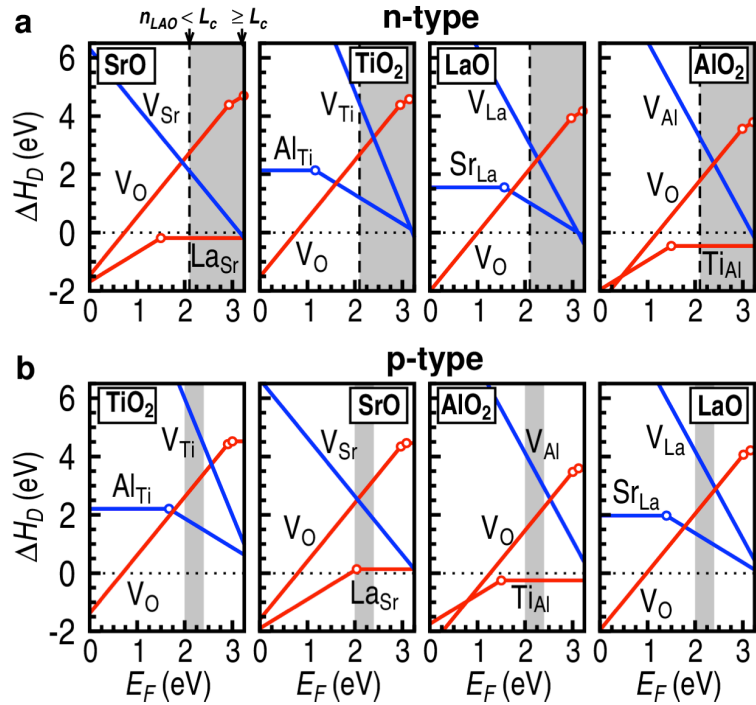


Figure 3: Properties of the interfacial point defects in the 6STO/2LAO heterostructure. **a,b**, the ΔH the interfacial defects at the n-type and p-type interface, respectively, as a function of the E_F . Each panel shows various defects in a given atomic layer. Each line represents the ΔH of a donor (red) or acceptor (blue) defect. Different slopes of line segments represent different charge states of a defect that are most stable at given E_F . Open circles mark the defect charge transition energies, i.e., the E_F where the formation energy of a defect in two different charge states equal. The shaded regions in each panel denote the variation range of the equilibrium E_F , resulting from interfacial point defects only. Other cation defects that have higher ΔH are shown in Extended Data Fig. 2. The chemical potentials for Sr, Ti, La, Al, and O are -4.36, -6.20, -6.10, -5.46, and -2.0 eV respectively, relative to their corresponding elemental solid or gas phases, which corresponds to $T=1050$ K and $P_{O_2} = 6.1 \times 10^{-6}$ Torr. To a large extent, the ΔH vs. E_F for a given defect at the same type of interfaces with different LAO thickness is similar since the defect has the same local bonding and electrostatic environments at the interface.

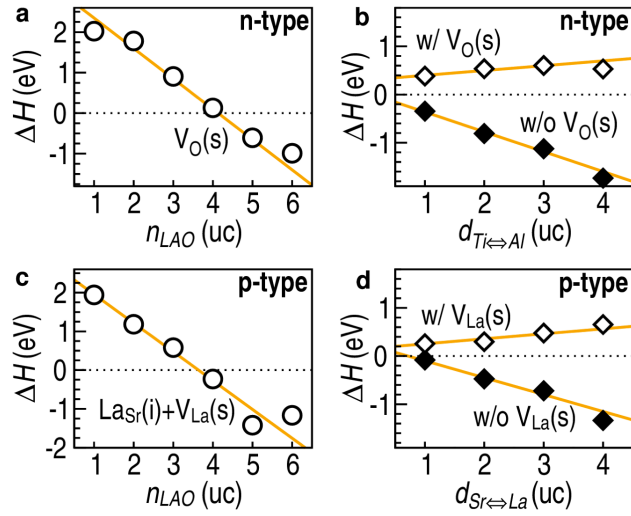


Figure 4: Properties of surface defects and defect complexes. **a**, the GGA-calculated ΔH of $V_O(s)$ defect, under the O-rich growth condition (i.e., $\Delta\mu_O = -1.5$ eV, Extended Data Fig. 1a). **b**, the ΔH of $[Ti_{Al}+Al_{Ti}]$ defect pair created from a $Ti \leftrightarrow Al$ exchange out of the ideal interface with and without a $V_O(S)$ in a 2×2 6STO/4LAO/vacuum supercell. **c**, the GGA-calculated ΔH of $[La_{Sr}(I)+V_{La}(S)]$ defect complex as a function of n_{LA0} , under $\Delta\mu_{Sr} = -4.36$ eV (Extended Data Fig. 1b). **d**, the ΔH of $[La_{Sr}+Sr_{La}]$ defect pair created from a $La \leftrightarrow Sr$ exchange out of the ideal interface with and without a $V_{La}(S)$ in a 2×2 6STO/4LAO/vacuum supercell, respectively. The $d_{Ti \leftrightarrow Al}$ and $d_{La \leftrightarrow Sr}$ in **b,d** are the distance from Al_{Ti} to $Al_{Ti}(I)$, and from Sr_{La} to $La_{Sr}(I)$, respectively. The orange lines are the guides to the eye.

References

- 1 Hwang, H. Y. *et al.* Emergent phenomena at oxide interfaces. *Nat Mater* **11**, 103-113 (2012).
- 2 Bogorin, D. F., Irvin, P., Cen, C., Levy, J. in *Multifunctional oxide heterostructures* (ed E.Y. Tsymbal, Gagotto, E.A., Eom, C., Ramesh R.) Ch. 13, 364 (Oxford University Press, 2012).
- 3 Mannhart, J. & Schlom, D. G. Oxide Interfaces-An Opportunity for Electronics. *Science* **327**, 1607-1611 (2010).
- 4 Ohtomo, A. & Hwang, H. Y. A high-mobility electron gas at the LaAlO₃/SrTiO₃ heterointerface. *Nature* **427**, 423-426 (2004).
- 5 Thiel, S., Hammerl, G., Schmehl, A., Schneider, C. W. & Mannhart, J. Tunable quasi-two-dimensional electron gases in oxide heterostructures. *Science* **313**, 1942-1945 (2006).
- 6 Brinkman, A. *et al.* Magnetic effects at the interface between non-magnetic oxides. *Nat Mater* **6**, 493-496 (2007).
- 7 Li, L., Richter, C., Mannhart, J. & Ashoori, R. C. Coexistence of magnetic order and two-dimensional superconductivity at LaAlO₃/SrTiO₃ interfaces. *Nat Phys* **7**, 762-766 (2011).
- 8 Kalisky, B. *et al.* Critical thickness for ferromagnetism in LaAlO₃/SrTiO₃ heterostructures. *Nat Commun* **3**, 922 (2012).
- 9 Salman, Z. *et al.* Nature of Weak Magnetism in SrTiO₃/LaAlO₃ Multilayers. *Phys Rev Lett* **109**, 257207 (2012).
- 10 Lee, J. S. *et al.* Titanium d(xy) ferromagnetism at the LaAlO₃/SrTiO₃ interface. *Nat Mater* **12**, 703-706 (2013).
- 11 Joshua, A., Ruhman, J., Pecker, S., Altman, E. & Ilani, S. Gate-tunable polarized phase of two-dimensional electrons at the LaAlO₃/SrTiO₃ interface. *P Natl Acad Sci USA* **110**, 9633-9638 (2013).
- 12 Ariando *et al.* Electronic phase separation at the LaAlO₃/SrTiO₃ interface. *Nat Commun* **2**, 188 (2011).
- 13 Reyren, N. *et al.* Superconducting interfaces between insulating oxides. *Science* **317**, 1196-1199 (2007).
- 14 Chakhalian, J., Millis, A. J. & Rondinelli, J. Whither the oxide interface. *Nat Mater* **11**, 92-94 (2012).
- 15 Chen, H. H., Kolpak, A. M. & Ismail-Beigi, S. Electronic and Magnetic Properties of SrTiO₃/LaAlO₃ Interfaces from First Principles. *Adv Mater* **22**, 2881-2899 (2010).
- 16 Nakagawa, N., Hwang, H. Y. & Muller, D. A. Why some interfaces cannot be sharp. *Nat Mater* **5**, 204-209 (2006).
- 17 Reinle-Schmitt, M. L. *et al.* Tunable conductivity threshold at polar oxide interfaces. *Nat Commun* **3**, 932 (2012).
- 18 Siemons, W. *et al.* Origin of charge density at LaAlO₃ on SrTiO₃ heterointerfaces: Possibility of intrinsic doping. *Phys Rev Lett* **98**, 196802 (2007).
- 19 Kalabukhov, A. *et al.* Effect of oxygen vacancies in the SrTiO₃ substrate on the electrical properties of the LaAlO₃/SrTiO₃ interface. *Phys Rev B* **75**, 121404 (2007).
- 20 Herranz, G. *et al.* High mobility in LaAlO₃/SrTiO₃ heterostructures: Origin, dimensionality, and perspectives. *Phys Rev Lett* **98**, 216803 (2007).
- 21 Cen, C. *et al.* Nanoscale control of an interfacial metal-insulator transition at room temperature. *Nat Mater* **7**, 298-302 (2008).
- 22 Zhong, Z. C., Xu, P. X. & Kelly, P. J. Polarity-induced oxygen vacancies at LaAlO₃/SrTiO₃ interfaces. *Phys Rev B* **82**, 165127 (2010).

23 Bristowe, N. C., Littlewood, P. B. & Artacho, E. Surface defects and conduction in polar oxide heterostructures. *Phys Rev B* **83**, 205405 (2011).

24 Li, Y., Phattalung, S. N., Limpijumnong, S., Kim, J. & Yu, J. Formation of oxygen vacancies and charge carriers induced in the n-type interface of a LaAlO₃ overlayer on SrTiO₃(001). *Phys Rev B* **84**, 245307 (2011).

25 Vonk, V. *et al.* Polar-discontinuity-retaining A-site intermixing and vacancies at SrTiO₃/LaAlO₃ interfaces. *Phys Rev B* **85**, 045401 (2012).

26 Gunkel, F. *et al.* Influence of charge compensation mechanisms on the sheet electron density at conducting LaAlO₃/SrTiO₃-interfaces. *Appl Phys Lett* **100**, 052103(2012).

27 Yamamoto, R. *et al.* Structural Comparison of n-Type and p-Type LaAlO₃/SrTiO₃ Interfaces. *Phys Rev Lett* **107**, 036104 (2011).

28 Qiao, L., Droubay, T. C., Kaspar, T. C., Sushko, P. V. & Chambers, S. A. Cation mixing, band offsets and electric fields at LaAlO₃/SrTiO₃(001) heterojunctions with variable La:Al atom ratio. *Surf Sci* **605**, 1381-1387 (2011).

29 Kalabukhov, A. S. *et al.* Cationic Disorder and Phase Segregation in LaAlO₃/SrTiO₃ Heterointerfaces Evidenced by Medium-Energy Ion Spectroscopy. *Phys Rev Lett* **103**, 146101 (2009).

30 Willmott, P. R. *et al.* Structural basis for the conducting interface between LaAlO₃ and SrTiO₃. *Phys Rev Lett* **99**, 155502 (2007).

31 Warusawithana, M. P. R., C.; Mundy, J. A.; Roy, P.; Ludwig, J.; Paetel, S.; Heeg, T.; Pawlicki, A. A.; Kourkoutis, L. F.; Zheng, M.; Lee, M.; Mulcahy, B.; Zander, W.; Zhu, Y.; Schubert, J.; Eckstein, J. N.; Muller, D. A.; Hellberg, C. S.; Mannhart, J.; Schlom, D. G. LaAlO₃ stoichiometry is key to electron liquid formation at LaAlO₃/SrTiO₃ interfaces. *Nat Commun* **4** (2013).

32 Fidkowski, L., Jiang, H. C., Lutchyn, R. M. & Nayak, C. Magnetic and superconducting ordering in one-dimensional nanostructures at the LaAlO₃/SrTiO₃ interface. *Phys Rev B* **87**, 014436 (2013).

33 Michaeli, K., Potter, A. C. & Lee, P. A. Superconducting and Ferromagnetic Phases in SrTiO₃/LaAlO₃ Oxide Interface Structures: Possibility of Finite Momentum Pairing. *Phys Rev Lett* **108**, 117003 (2012).

34 Pavlenko, N., Kopp, T., Tsymbal, E. Y., Mannhart, J. & Sawatzky, G. A. Oxygen vacancies at titanate interfaces: Two-dimensional magnetism and orbital reconstruction. *Phys Rev B* **86**, 064431 (2012).

35 Lany, S. & Zunger, A. Assessment of correction methods for the band-gap problem and for finite-size effects in supercell defect calculations: Case studies for ZnO and GaAs. *Phys Rev B* **78**, 235104 (2008).

36 Van de Walle, C. G. & Neugebauer, J. First-principles calculations for defects and impurities: Applications to III-nitrides. *J Appl Phys* **95**, 3851-3879 (2004).

37 Chambers, S. A. *et al.* Instability, intermixing and electronic structure at the epitaxial LaAlO₃/SrTiO₃(001) heterojunction. *Surf Sci Rep* **65**, 317-352 (2010).

38 Zhang, L. X. *et al.* Origin of insulating behavior of the p-type LaAlO₃/SrTiO₃ interface: Polarization-induced asymmetric distribution of oxygen vacancies. *Phys Rev B* **82**, 125412 (2010).

39 Xie, Y. W., Hikita, Y., Bell, C. & Hwang, H. Y. Control of electronic conduction at an oxide heterointerface using surface polar adsorbates. *Nat Commun* **2**, 494 (2011).

40 Son, W. J., Cho, E., Lee, J. & Han, S. Hydrogen adsorption and carrier generation in LaAlO₃-SrTiO₃ heterointerfaces: a first-principles study. *J Phys-Condens Mat* **22**, 315501 (2010).

41 Bi, F. *et al.* "Water-cycle" mechanism for writing and erasing nanostructures at the LaAlO₃/SrTiO₃ interface. *Appl Phys Lett* **97**, 173110 (2010).

42 Arras, R., Ruiz, V. G., Pickett, W. E. & Pentcheva, R. Tuning the two-dimensional electron
gas at the LaAlO₃/SrTiO₃(001) interface by metallic contacts. *Phys Rev B* **85**, 125404
(2012).

43 Perdew, J. P., Burke, K. & Ernzerhof, M. Generalized gradient approximation made simple.
Phys Rev Lett **77**, 3865-3868 (1996).

44 Lee, J. & Demkov, A. A. Charge origin and localization at the n-type SrTiO₃/LaAlO₃
interface. *Phys Rev B* **78**, 193104 (2008).

45 Perdew, J. P. & Levy, M. Physical Content of the Exact Kohn-Sham Orbital Energies - Band-
Gaps and Derivative Discontinuities. *Phys Rev Lett* **51**, 1884-1887(1983).

46 Heyd, J., Scuseria, G. E. & Ernzerhof, M. Hybrid functionals based on a screened Coulomb
potential (vol 118, pg 8207, 2003). *J Chem Phys* **124**, 219906 (2006).

47 Cossu, F., Schwingenschlogl, U. & Eyert, V. Metal-insulator transition at the LaAlO₃/SrTiO₃
interface revisited: A hybrid functional study. *Phys Rev B* **88**, 045119 (2013).

48 Dingle, R., Stormer, H. L., Gossard, A. C. & Wiegmann, W. Electron Mobilities in Modulation-
Doped Semiconductor Heterojunction Super-Lattices. *Appl Phys Lett* **33**, 665-667 (1978).

49 Pentcheva, R. & Pickett, W. E. Avoiding the Polarization Catastrophe in LaAlO₃ Overlayers
on SrTiO₃(001) through Polar Distortion. *Phys Rev Lett* **102**, 107602 (2009).

50 Segal, Y., Ngai, J. H., Reiner, J. W., Walker, F. J. & Ahn, C. H. X-ray photoemission studies of
the metal-insulator transition in LaAlO₃/SrTiO₃ structures grown by molecular beam
epitaxy. *Phys Rev B* **80**, 241107 (2009).

51 Huang, B. C. *et al.* Mapping Band Alignment across Complex Oxide Heterointerfaces. *Phys
Rev Lett* **109**, 246807 (2012).

52 Slooten, E. *et al.* Hard x-ray photoemission and density functional theory study of the
internal electric field in SrTiO₃/LaAlO₃ oxide heterostructures. *Phys Rev B* **87**, 085128
(2013).

53 Berner, G. *et al.* Band alignment in LaAlO₃/SrTiO₃ oxide heterostructures inferred from
hard x-ray photoelectron spectroscopy. *Phys Rev B* **88**, 115111 (2013).

54 Son, W. J., Cho, E., Lee, B., Lee, J. & Han, S. Density and spatial distribution of charge
carriers in the intrinsic n-type LaAlO₃-SrTiO₃ interface. *Phys Rev B* **79**, 245411 (2009).

55 Popovic, Z. S., Satpathy, S. & Martin, R. M. Origin of the Two-Dimensional Electron Gas
Carrier Density at the LaAlO₃ on SrTiO₃ Interface. *Phys Rev Lett* **101**, 256801 (2008).

56 Delugas, P. *et al.* Spontaneous 2-Dimensional Carrier Confinement at the n-Type
SrTiO₃/LaAlO₃ Interface. *Phys Rev Lett* **106**, 166807 (2011).

57 Seo, S. S. A. *et al.* Multiple conducting carriers generated in LaAlO₃/SrTiO₃
heterostructures. *Appl Phys Lett* **95**, 082107 (2009).

58 Moetakef, P. *et al.* Electrostatic carrier doping of GdTiO₃/SrTiO₃ interfaces. *Appl Phys Lett*
99, 232116 (2011).

59 Sato, H. K., Bell, C., Hikita, Y. & Hwang, H. Y. Stoichiometry control of the electronic
properties of the LaAlO₃/SrTiO₃ heterointerface. *Appl Phys Lett* **102**, 251602 (2013).

60 Takizawa, M., Tsuda, S., Susaki, T., Hwang, H. Y. & Fujimori, A. Electronic charges and
electric potential at LaAlO₃/SrTiO₃ interfaces studied by core-level photoemission
spectroscopy. *Phys Rev B* **84**, 245124 (2011).

61 Koitzsch, A. *et al.* In-gap electronic structure of LaAlO₃-SrTiO₃ heterointerfaces
investigated by soft x-ray spectroscopy. *Phys Rev B* **84**, 245121 (2011).

62 Pentcheva, R. & Pickett, W. E. Charge localization or itineracy at LaAlO₃/SrTiO₃ interfaces:
Hole polarons, oxygen vacancies, and mobile electrons. *Phys Rev B* **74**, 035112 (2006).

63 Blochl, P. E. Projector Augmented-Wave Method. *Phys Rev B* **50**, 17953-17979 (1994).

64 Kresse, G. & Furthmuller, J. Efficiency of ab-initio total energy calculations for metals and
semiconductors using a plane-wave basis set. *Comp Mater Sci* **6**, 15-50 (1996).

65 Yu, L. P., Ranjan, V., Lu, W., Bernholc, J. & Nardelli, M. B. Equivalence of dipole correction
and Coulomb cutoff techniques in supercell calculations. *Phys Rev B* **77**, 245102 (2008).

66 Yu, L. P., Ranjan, V., Nardelli, M. B. & Bernholc, J. First-principles investigations of the
dielectric properties of polypropylene/metal-oxide interfaces. *Phys Rev B* **80**, 165432
(2009).

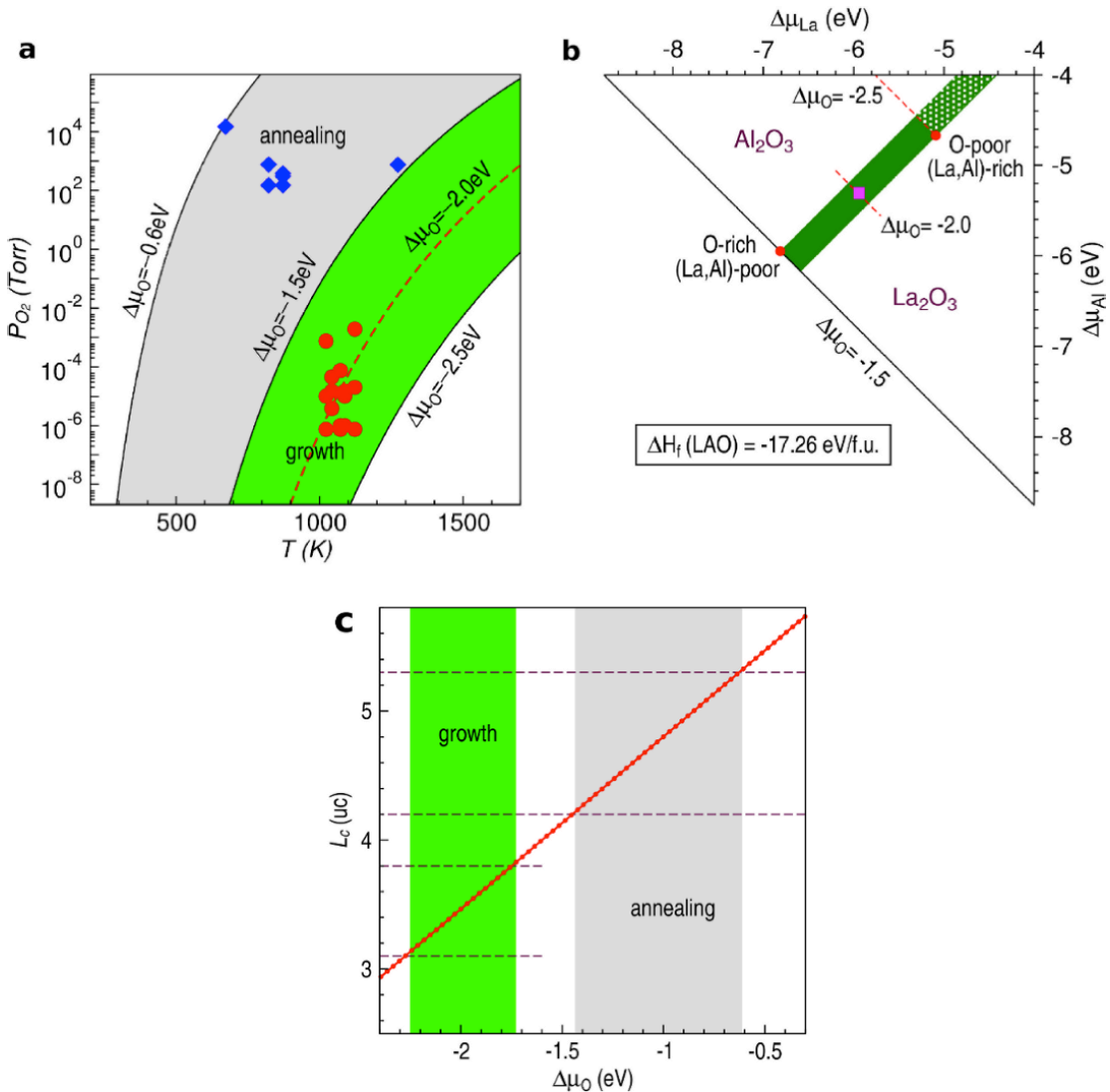
67 Persson, C., Zhao, Y. J., Lany, S. & Zunger, A. n-type doping of CuInSe₂ and CuGaSe₂. *Phys
Rev B* **72**, 035211 (2005).

68 Osorio-Guillen, J., Lany, S., Barabash, S. V. & Zunger, A. Magnetism without magnetic ions:
Percolation, exchange, and formation energies of magnetism-promoting intrinsic defects
in CaO. *Phys Rev Lett* **96**, 107203 (2006).

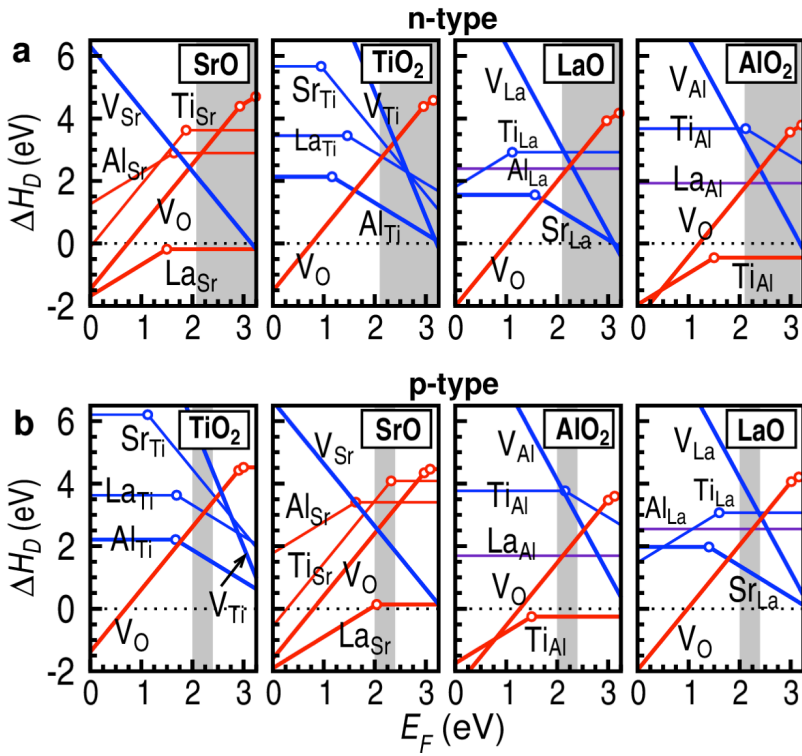
Extended Data Table 1: List of the important experimental observations pertaining to LAO/STO interfaces.

Interface structure	Expt. Observations	Polar Catastrophe	Cation Mixing	Interfacial V_0	Surface V_0	Current Mechanism
n-type	N1. Critical thickness (L_c): 4 uc	?	✗	?	?	✓
	N2. $E \sim 0$ in LAO for $n_{LAO} < L_c$	✗	?	✗	✗	✓
	N3. $E \sim 0$ in LAO for $n_{LAO} \geq L_c$	✗	✗	✗	✓	✓
	N4. Interface: cation mixed	✗	✓	✗	✗	✓
	N5. Interface: in-gap states exist	✗	?	✗	✗	✓
	N6. Interface: Ti^{3+} found below L_c	✗	?	✗	✗	✓
	N7. Local magnetic moment	✗	?	?	✗	✓
	N8. Reduced carrier density $\sim 10^{13} \text{ cm}^{-2}$	✗	?	✗	✗	✓
	N9. Interfacial Q_e depends on P_{O2}	✗	✗	✓	✓	✓
	N10. LAO surface: insulating ^b	✗	?	?	✓	✓
p-type	P1. Interface: cation mixed	✗	✓	✗	✗	✓
	P2. Interface: insulating	✗	?	?	?	✓
	P3. LAO surface: insulating	✗	?	?	?	✓

The symbol of ‘✓’ and ‘✗’ mean that the proposed mechanism agrees or disagrees, respectively with experimental observation. The ‘?’ symbol denotes uncertainty. Q_e is the measured interfacial carrier density from transport.



Extended Data Figure 1: Thermodynamic equilibrium growth conditions and critical thickness for STO/LAO interface. **a**, typical growth (circles) and annealing (diamonds) conditions vs. oxygen chemical potential $\Delta\mu_O$ defined relative to O_2 molecule. The $\Delta\mu_O$ that corresponds to the experimental (P_{O_2} , T) growth conditions was calculated according to the thermodynamic model in Ref.1. The red dashed line corresponds to $T = 1050\text{ K}$ and $P_{O_2} = 6.1 \times 10^{-6}\text{ Torr}$, which is referred in Fig.3c,d. **b**, allowed equilibrium chemical potentials (green area) for growing LAO film on top of STO substrate. Under equilibrium, the chemical potentials of elements satisfy $\Delta\mu_{\text{La}} + \Delta\mu_{\text{Al}} + \Delta\mu_O = \Delta H_f = -17.26\text{ eV}$. The experimental condition used for Fig.3 refer to $\Delta\mu_O = -2.0\text{ eV}$. **c**, the critical thickness (L_c) as a function of O chemical potential used during growth and annealing process (See supplementary discussion).



Extended Data Figure 2: Properties of interfacial defects in the 6STO/2LAO heterostructure containing both n-type and p-type interfaces. Same as Fig. 3, but includes other defects with higher formation energies. **a**, n-type interface. **b**, p-type interface. Each panel in **a,b** shows various defects in a given atomic layer. Each line represents the ΔH of a donor (red) or acceptor (blue) defect. Different slopes of line segments represent different charge states of a defect that are most stable at given E_F . Open circles mark the defect charge transition energies, i.e., the E_F where the formation energy of a defect in two different charge states equal. The shaded regions in each panel denote the variation range of the equilibrium E_F . The chemical potentials for Sr, Ti, La, Al, and O are -4.36, -6.20, -6.10, -5.46, and -2.0 eV respectively, relative to their corresponding elemental solid or gas phases, which corresponds to $T=1050$ K and $PO_2 = 6.1 \times 10^{-6}$ Torr.

Supplementary Information

Supplementary Discussion

1. On the slope of “ ΔH vs n_{LAO} ” line in Fig.4:

In a supercell calculation, the formation energy of an oxygen vacancy at LAO surface (denoted as V_O (*s*) hereafter) is

$$\Delta H = [\mathcal{E}_D^0 + en_{LAO}E'] - [\mathcal{E}_H^0 + en_{LAO}E] + \mu_O, \quad (1)$$

where \mathcal{E}_D^0 and \mathcal{E}_H^0 are the total energies of the supercell structures in the absence of an electric field across the LAO film with and without the vacancy. The second term in each of the brackets corresponds to the electrostatic energy rise due to the presence of internal electric field E' and E in LAO with and without V_O , respectively. In a 2×2 2D supercell considered here the creation of a single V_O (*S*) leads to zero electric field in LAO ($E' = 0$ for all n_{LAO}).^{21,24,34} Therefore, Eq. (1) reduces to $\Delta H = [\mathcal{E}_D^0 - \mathcal{E}_H^0 + \mu_O] - en_{LAO}E$, where the second term can now be viewed as an opposite dipole, which decreases linearly at a rate of eE as n_{LAO} increases.

2. On the critical thickness vs oxygen chemical potential in Extended Figure 2b:

Eq.(1) suggests that the critical L_c can be approximately determined by the ΔH of the interfacial V_O in TiO_2 layer and the electric field E in the defect-free LAO film (from electrostatics), via

$$L_c = [\mathcal{E}_D^0 - \mathcal{E}_H^0 + \mu_O]/eE, \quad (2)$$

which is a function of the oxygen chemical potential μ_O and the built-in electric field in defect-free LAO. Extended Figure 1b shows the variation of resulting L_c due to V_O (*S*) with respect to $\Delta\mu_O$ (i.e., the oxygen chemical potential relative to $1/2O_2$) at $T = 0K$. The corresponding $\Delta\mu_O$ of current growth conditions ranges from -1.73 to -2.25 eV, where the L_c is found to be between 3.1 and 3.8 uc. The O-rich annealing conditions have $\Delta\mu_O$ ranging from -0.61 to -1.44 eV, where the resulting L_c varies from 4.2 to 5.3 uc. Considering the possible high kinetic barrier associated with the low-temperature annealing, the O vacancies induced during the growth generally may not be completely compensated, and thus it is expected that the actually L_c in the annealed samples be ~ 4 uc, consistent with experiments.